FOUR-DIMENSIONAL FUEL-OPTIMAL FLIGHTS INTO AND OUT OF THE TERMINAL AREA

H.G. Visser
Faculty of Aerospace Engineering
Delft University of Technology
Delft, The Netherlands

Abstract

The problem of four-dimensional fuel-optimal flight into and out of a terminal area is studied using a reduced-order (energy state) system formulation. The Minimum Principle of Optimal Control Theory is employed to generate climb-out and descent extremals (turning and nonturning) in the form of a three-parameter family. Extremals that pass through specified end conditions at a specified time can be obtained by searching in the three-dimensional parameter-space. The trajectory-family structure allows significant insight into the energy management features of four-dimensional fuel-optimal flight. Numerical examples are given to illustrate these energy management features, as well as to quantify the penalties in fuel consumption which result from operational (ATC) constraints.

I. Introduction

Aircraft approaching a high density Terminal Area (TMA) are often confronted with unforeseen delays. In order to absorb such time delays, ATC generally enforces route extensions or holdings, which obviously results in a significant waste of fuel. Time-based traffic management procedures hold the key to solving such problems by assigning each arriving aircraft a landing time as early as possible. Indeed, if a reassigned arrival time can be made available early during the flight, then revised trajectories can be generated to absorb time in a fuel-efficient manner. These potential fuel-savings have spurred a considerable research interest into Four-Dimensional (4-D) guidance systems in recent years. The feasibility of 4-D guidance algorithms has already been demonstrated in experimental investigations, however, the main focus was on time-based metering rather than on fuel-optimality [1].

By specifying total fuel consumption as the Performance Index, the 4-D terminal area trajectory problem can be analyzed as a fixed-time Optimal Control problem. Unfortunately, however, application of Optimal Control Theory to a point-mass-vehicle dynamic model results in a Two-Point-Boundary-Value Problem (TPBVP) which is known to be of a formidable computational complexity. For this reason, reduced-order concepts, in which dynamics that are believed to have little effect on the solution behavior are neglected, have received considerable attention.

The earliest and best-known reduced-order concept is that of energy-state [2]. This concept makes use of total energy as a state variable and reductions of model-order by ignoring altitude and path-angle dynamics. In the area of transport aircraft performance optimization, energy-state

approximations along the lines of Erzberger et. al. [3] have formed the basis for fuel savings systems on many commercial aircraft. In more recent studies involving flight in a vertical plane, Erzberger's energy state approximation was extended to include a fixed time-of-arrival [4,5,6].

Terminal-area minimum-fuel climb-out and descent problems are rather difficult to solve, because vertical and horizontal maneuvers involving speed, altitude and heading changes, which are all of comparable significance in influencing fuel-consumption, occur simultaneously. This precludes model-order reductions beyond a fourth-order system, if the most important dynamic effects are to be taken into account. For this reason, the analysis of terminal area maneuvers based on complete three-dimensional problem formulations has received modest attention only. In Refs. 7 and 8, time-free minimum-fuel three-dimensional flight paths have been computed using a performance model intermediate in complexity between the energy-state and full-order point mass vehicle models. However, only representative flight paths below 10,000 ft altitude have been generated using an extremal field approach.

This paper documents the outcome of a research effort in which the terminal area trajectory optimization problem is treated in reduced-order approximation, using the fourth-order "energy-state" system model of Ref.2. Since the capability to absorb time is proportional to how long in advance the arrival time is known, an extended Terminal Area (200-250 km) was considered, motivated by the so-called "Zone of Convergence" concept of Benoit et. al. [9]. Realistic propulsion and aerodynamic models, representative of a jet transport, have been used in the computations. In addition, the most important performance and operational (ATC) constraints have been taken in account.

Representative climb-out and descent trajectories can be generated in the form of a three-parameter family. Two-Point-Boundary-Value Problems are then solved by performing a search in this three-dimensional parameter-space.

The present investigations are essentially theoretical in nature and primarily aimed at obtaining insight into the energy management features of 4-D fuel-optimal flight. Indeed, the observed structure of trajectory-families allows the essential energy management features, i.e., the characteristics that provide most of the fuel savings, to be identified. Eventually, this insight may be beneficially exploited in the development of sub-optimal algorithms that can be implemented on board. The current investigation provides standards against which such developments can be evaluated. In addition, it is possible to assess the penalties in fuel consumption which are brought about by operational (ATC) constraints.

II. Optimal Control Formulation

Equations of Motion

The three-dimensional energy-state model is described by the following equations [2,10]:

$$\dot{x} = V \cos X \tag{1}$$

$$\dot{y} = V \sin X \tag{2}$$

$$\dot{E} = V(T - D)/W \tag{3}$$

$$\dot{X} = (g/V)L\sin\mu/W \tag{4}$$

Here the states are, x and y the position coordinates in the horizontal plane, E the specific energy and X the heading angle. It is assumed that the aerodynamic forces have the form:

$$L(h,V,C_L) = C_L qS \tag{5}$$

$$D(h,V,C_L) = \left(C_{D_0}(M) + K(M)C_L^2 + \xi\Delta C_D \right)qS , \tag{6}$$

where ξ is the speedbrake setting and $\xi\Delta C_D$ accounts for the speedbrake incremental drag. The equations of motion embody the assumptions of a constant-weight vehicle with thrust directed along the flight path and coordinated turns. The condition of force equilibrium in the vertical plane, which results from the order-reduction (i.e., neglecting the path angle dynamics), relates the lift coefficient C_L to the bank angle μ through:

$$(C_L qS)\cos\mu = W \tag{7}$$

The thrust T is constrained to be between idle and maximum allowable settings:

$$T_{min}(M,h) \leq T \leq T_{max}(M,h) \tag{8}$$

The throttle setting η, defined as:

$$\eta = \frac{T - T_{min}}{T_{max} - T_{min}} , \tag{9}$$

is introduced to serve as one of the aircraft's control variables. Thrust T in Eq.(3) can then be written as:

$$T = \eta\left(T_{max}(M,h) - T_{min}(M,h) \right) + T_{min}(M,h) \tag{10}$$

Obviously the permissible range of η is $0 \leq \eta \leq 1$. The three remaining control variables are bank angle μ , altitude h and speedbrake setting ξ (also with permissible range, $0 \leq \xi \leq 1$). Airspeed V is to be merely regarded as a function of control h and state E:

$$V = \left(2g(E-h) \right)^{1/2} \tag{11}$$

The inequality constraints on the state and control variables are specified by:

$$\beta_1 = h - h_T \geq 0 \qquad \text{(terrain limit)} \tag{12}$$

$$\beta_2 = q_{MO} - q \geq 0 \qquad (V_{MO} \text{ limit}) \tag{13}$$

$$\beta_3 = M_{MO} - M \geq 0 \qquad (M_{MO} \text{ limit}) \tag{14}$$

$$\beta_4 = \cos\mu - W/(qSC_{L_{max}}) \geq 0 \text{ (lift limit)} \tag{15}$$

$$\beta_5 = \cos\mu - \cos\mu_{max} \geq 0 \qquad \text{(bank angle limit)} \tag{16}$$

$$\beta_6 = \eta(1 - \eta) \geq 0 \qquad \text{(throttle setting limits)} \tag{17}$$

$$\beta_7 = \xi(1 - \xi) \geq 0 \qquad \text{(speedbrake setting limits)} \tag{18}$$

In addition to the constraints (12) through (18), there are also operational constraints involving the flight path angle (or rate of climb/descent). Unfortunately, however, these constraints can not be directly enforced, simply because flight path angle is not a variable in the energy-state model. However, it is possible to examine possible violations of these constraints a posteriori, once the solution in the (V,h)-space has been established. Moreover, these constraints can be imposed indirectly by introducing additional constraints in the (V,h)-space.

Figure 1 shows several of the constraints in the (V,h)-space for the aircraft model used in the numerical examples. The aircraft model concerns a Lockheed C-141 type of jet transport [11]. A description of this model, a modified version of the model of Ref.12, is given in the Appendix.

Also shown in Figure 1 is the FAA imposed constraint which states that the indicated airspeed in the terminal area must not exceed 250 kts, below an altitude of 10,000 ft. This constraint has been enforced in some of the numerical examples.

The so-called "corner-velocity" locus indicated in Figure 1, will play an important part in the analysis that follows. The corner velocity is defined as the velocity at a given energy level at which the constraints in Eqs.(15) and (16) are met simultaneously:

$$V_c(E) = \left(2W/(\rho SC_{L_{max}} \cos\mu_{max}) \right) \tag{19}$$

The significance of the corner-velocity locus is two-fold. Firstly, this curve represents the locus of maximum instantaneous turn rate. Secondly, this curve separates two distinct regions in the (V,h)-space: to the left of the locus the lift coefficient is constrained by the lift limit; to the right of the locus the lift coefficient is limited by the maximum allowable bank angle.

The loft ceiling indicated in Figure 1, represents the maximum altitude that can be attained at any given energy level, without violating the lift limit in Eq.(15).

Problem Statement

The equations of motion are written in a coordinate frame that has its origin at the entry point (descent) or exit point (climb-out) at the boundary of the TMA. For the descent this is illustrated in Figure 2. Within the context of the current investigation, descent flight paths are those flight paths that start at the TMA boundary (entry fix) from a specified cruise energy level and that end on the centerline extension of the approach runway (metering fix) with the proper final heading, energy and time-of-arrival. The orientation of the reference frame is such that the line connecting the entry fix and the metering fix has a *direction* relative to the *x*-axis (see Figure 2):

$$\chi_m = \arctan\left[y(t_f)/x(t_f)\right] \qquad (20)$$

Since the final cross-range is generally very small compared to the final down-range (typically, $\chi_m < 1°$), the assumption $x_f \approx R$ seems justified, where R is the radius of the extended TMA.

The optimal descent problem to be solved is thus to determine the controls η, ξ, μ, h such that starting from the initial conditions:

$$x(t_0) = 0 , \quad y(t_0) = 0 , \quad E(t_0) = E_{cr} \qquad (21)$$

the aircraft reaches the final conditions:

$$x(t_f) = R , \quad E(t_f) = E_f , \quad \chi(t_f) = \chi_f , \qquad (22)$$

while minimizing the total fuel consumption:

$$J = W_F(t_f) = \int_{t_0}^{t_f} \sigma(h,M,T) \, dt , \qquad (23)$$

where t_f is the assigned arrival time. The fuel flow rate σ is modeled by [12]:

$$\sigma(h,M,T) = K_1(M,h) + K_2(M,h)T + K_3(M,h)T^2 \qquad (24)$$

At this stage it is noted that neither the initial heading $\chi(t_0)$ nor the final cross-range $y(t_f)$ are specified as *boundary conditions*. The reason for this particular problem formulation will become apparent in subsequent analysis.

The optimal climb-out problem can be formulated in an entirely analogous fashion. It is obvious, however, that the initial and terminal boundary conditions in Eqs.(21) and (22) need to be "switched":

$$x(t_0) = -R , \quad E(t_0) = E_0 , \quad \chi(t_0) = \chi_0 \qquad (25)$$

$$x(t_f) = 0 , \quad y(t_f) = 0 , \quad E(t_f) = E_{cr} , \qquad (26)$$

Note that, in contrast to the descent problem formulation, the x-axis of the reference frame is pointing <u>outward</u> in the climb-out problem.

Necessary Conditions for Optimality

The variational Hamiltonian can be formed in the usual fashion [13]:

$$H = \sigma + \lambda_x V\cos\chi + \lambda_y V\sin\chi + \lambda_E V(T - D)/W + \lambda_\chi(g/V)\tan\mu \qquad (27)$$

In order to facilitate treatment of the inequality constraints by the technique of Valentine, the augmented Hamiltonian is introduced [2]:

$$\bar{H} = H + \sum_{j=1}^{7} \lambda_j \beta_j , \qquad (28)$$

where the λ_j's are multipliers satisfying the conditions:

$$\lambda_j < 0, \text{ if } \beta_j = 0$$

$$\lambda_j = 0, \text{ if } \beta_j > 0 , \quad j = 1,\dots,7 \qquad (29)$$

The necessary conditions of optimality include the adjoint equations:

$$\dot{\lambda}_x = -\frac{\partial \bar{H}}{\partial x} = 0 \qquad (30)$$

$$\dot{\lambda}_y = -\frac{\partial \bar{H}}{\partial y} = 0 \qquad (31)$$

$$\dot{\lambda}_\chi = -\frac{\partial \bar{H}}{\partial \chi} = \lambda_x V\sin\chi - \lambda_y V\cos\chi \qquad (32)$$

$$\dot{\lambda}_E = -\frac{\partial \bar{H}}{\partial E} = -\frac{\partial\sigma}{\partial E} - \lambda_x(g/V)\cos\chi - \lambda_y(g/V)\sin\chi -$$
$$- \lambda_E(g/V)(T - D)/W - \lambda_E(V/W)\frac{\partial(T-D)}{\partial E} +$$
$$+ \lambda_\chi(g^2/V^3)\tan\mu - \sum_{j=2}^{4} \lambda_j \frac{\partial\beta_j}{\partial E} \qquad (33)$$

It is worth noting that only three multipliers actually enter the adjoint equations.

The unspecified boundary conditions lead to the following transversality conditions:

$$\lambda_y(t_f) = 0 , \quad \lambda_\chi(t_0) = 0 \qquad \text{(descent)}$$

$$\lambda_y(t_0) = 0 , \quad \lambda_\chi(t_f) = 0 \qquad \text{(climb-out)} \qquad (34)$$

A substantial simplification of the TPBVP is obtained by closed form integration of the adjoint Eqs.(30)-(32). Using the boundary and transversality conditions, the following expressions result [14]:

$$\lambda_x = \text{Constant} , \quad \lambda_y = 0 , \quad \lambda_\chi = \lambda_x y \qquad (35)$$

The Minimum Principle can be used to express the optimal controls in terms of the state and adjoint

variables. The conditions determining the optimal controls and the multipliers are:

$$\frac{\partial \bar{H}}{\partial \eta} = 0 \ , \ \frac{\partial \bar{H}}{\partial \xi} = 0 \ , \ \frac{\partial \bar{H}}{\partial \mu} = 0 \ , \ \frac{\partial \bar{H}}{\partial h} = 0 \qquad (36)$$

For the optimal throttle setting, the first expression in Eq.(36) leads to:

$$\eta^* = 1 \quad \text{if } \eta_u \geq 1$$
$$ = \eta_u \quad \text{if } 0 < \eta < 1$$
$$ = 0 \quad \text{if } \eta_u \leq 0 \ , \qquad (37)$$

where:

$$\eta_u = -\frac{K_2 + 2K_3 T_{min} + \lambda_E(V/W)}{2K_3(T_{max} - T_{min})} \qquad (38)$$

It is readily observed that, since both K_2 and K_3 are greater than zero, interior throttle setting $\eta = \eta_u$ can only occur if $\lambda_E < 0$. Moreover, if $\lambda_E > 0$, the optimal throttle setting must be: $\eta = 0$.

The optimal speedbrake setting is found from the second expression in Eq.(36):

$$\xi^* = 1 \quad \text{if } \lambda_E > 0$$
$$ = 0 \quad \text{if } \lambda_E < 0 \ , \qquad (39)$$

The extremal bank angle is found by minimizing H with respect to μ and is given by:

$$\mu^* = \bar{\mu} \quad \text{if } \mu_u \geq \bar{\mu} \ \text{ and } \ \lambda_E < 0$$
$$ = \mu_u \quad \text{if } -\bar{\mu} < \mu < \bar{\mu} \ \text{ and } \ \lambda_E < 0$$
$$ = -\bar{\mu} \quad \text{if } \mu_u \leq -\bar{\mu} \ \text{ and } \ \lambda_E < 0$$
$$ = \bar{\mu} \ \text{sign}(\lambda_\chi) \quad \text{if } \lambda_E > 0 \ \text{ and } \ \lambda_\chi \neq 0 \qquad (40)$$

where:

$$\mu_u = \frac{\lambda_\chi \rho g}{4\lambda_E(W/S)K} \qquad (41)$$

$$\bar{\mu} = \min \left[\arccos\left(W/(qSC_{L_{max}})\right), \mu_{max}\right] \qquad (42)$$

The case $\lambda_E > 0$ and $\lambda_\chi = 0$ is special, due to the convexity condition that is violated [2,7,8]. This nonconvexity can be removed by allowing a so-called "relaxed control", i.e., a chattering bank angle $\mu(t)$, oscillating at infinite frequency between $-\bar{\mu}$ and $+\bar{\mu}$ in such a way that a nonturning flight path results. Although chattering is hardly practical, it makes sense from an optimal control point of view in situations which call for maximum

drag at zero thrust (recall that $\eta^* = 0$ and $\xi^* = 1$, if $\lambda_E > 0$) to achieve maximum deceleration. Another approach to resolve violations of the convexity condition is by introducing additional artificial constraints [7]. Although this approach avoids the need for relaxed control, it decreases the performance. This approach has not been pursued here.

At each point on the trajectory, the altitude that minimizes H is found by a numerical one-dimensional search. The analytic expressions that have been derived for the three remaining extremal controls facilitate this possibility. It is noted that the minimum of H as a function of h will often exhibit a "cusp", when it occurs at an altitude corresponding to the corner-velocity. Consequently, the numerical search should be performed with grate care. There are generally four possibilities for a minimum of H at a given energy level: at the upper altitude limit (loftceiling), at the corner-velocity locus, at an interior minimum ($\partial H/\partial h = 0$) or at the lower altitude limit (which can be either the terrain limit, the dynamic pressure limit, or the Mach limit). The value of h that gives the global minimum of H is taken as the extremal altitude.

The calculation of the multipliers λ_j from Eqs.(33) using the Valentine technique, is certainly not trivial. In particular, the calculation of these multipliers is complicated by the fact that some of the constraints can be active simultaneously [2].

III. Numerical Results

Calculation of Extremals

Extremals can be computed by numerical integration of the fifth-order system, consisting of the state Eqs.(1) through (4) and the adjoint Eq.(33), using the extremal controls derived in the previous section and starting at the appropriate boundary conditions.

The computation of descent extremals requires the specification of the "missing" initial values:

$$\chi(t_0) \ , \quad \lambda_E(t_0) \ , \quad \lambda_\chi(t_0) \qquad (43)$$

Descent trajectories can then be generated by integrating the fifth-order system _forward_ in time, starting at the initial (cruise) conditions (21).

Climb-out trajectories can be obtained in a similar fashion, however, now the system is integrated _backward_ in time, starting at the terminal (cruise) conditions (26). Climb-out trajectories are thus found as functions of time-to-go, with each extremal specified by the triplet:

$$\chi(t_f) \ , \quad \lambda_E(t_f) \ , \quad \lambda_\chi(t_f) \qquad (44)$$

Figures 3 and 4 show a typical family of descent extremals. Only one parameter of the triplet (43) is actually varied, namely the initial heading angle. If the initial heading angle is chosen identically zero, a _nonturning_ flight path results. This is not really a surprising result. Substitution of the transversality condition (34) in the control Eqs.(40) and (41), shows that for $\lambda_E < 0$:

$$\mu(t_0) = \dot{X}(t_0) = \lambda_\chi(t_0) = 0 \qquad (45)$$

If in addition the initial heading angle is selected as identically zero, we have from Eq.(32) that:

$$\dot{\lambda}_\chi(t_0) = 0 \qquad (46)$$

Consequently, bank angle and heading angle will remain identically zero along the extremal flight path. It is noted that a significant part of the trajectory is flown at idle thrust.

The turning members of the trajectory family in the Figures 3 and 4 (obtained by extremely small variations in the initial heading angle) all reveal a similar behavior: starting from the entry point the trajectories closely follow the central, nonturning, member of the family, but, when the turn is initiated altitude increases until the corner velocity locus is reached. The trajectories will subsequently "ride" the corner-velocity locus, with heading increasing and energy decreasing. Obviously, an extremal may follow one of the lower altitude constraints for some period of time. In figure 3, for example, one of the extremals follows the terrain limit for a period of time.

The results clearly indicate that turning should generally be performed at low altitude. The behavior of altitude during the turning phase is fairly transparent. If the emphasis in the optimization process is to be shifted towards high turning rates, the control actions are such that the flight is directed towards the corner-velocity locus, where the instantaneous turn rate is maximal.

The ground tracks shown in Figure 4 make clear how sensitive the system actually is to small variations in the initial heading angle. It is worth noting that the extremals are symmetric with respect to the x-axis for positive and negative values of the initial heading angle. Since extremals with a heading change larger than 180^0 are generally not globally optimal [10], turns are limited to a heading change of $\pm 180^0$ in the present analysis.

In figure 5, a climb-out trajectory-family is shown. It is recalled that climb-out extremals are obtained by retrograde integration (i.e. in a direction opposite of that of the arrows). The energy management features of the climb-out trajectory-family are not essentially different from those of the descent family. Similar to the descent profiles, climb-out trajectories are generally characterized by a turn at low altitude, flown at or near the corner-velocity locus. Despite the fact that full thrust is applied, the energy rate can be negative during this initial turn. This is also illustrated in Figure 6.

TPBVP Solutions

Due to the noted sensitivity of the state-Euler system, finding the extremal that exactly passes through the specified boundary conditions is generally a cumbersome computational task. Fortunately, however, by formulating the optimal control problem in the special form presented herein, this task could be significantly alleviated. This special problem formulation entails such aspects as location and orientation of the reference frame, specification of boundary conditions and closed form integration of some of the adjoint equations. In the present effort, Two-Point-Boundary-Value Problems are solved using a shooting method.

Descent trajectories are obtained by integrating the state-Euler system forward in time, starting with guessed values for the triplet in Eq.(43) and terminating when the assigned time of arrival has been reached. The guessed values are then iteratively adjusted until the terminal conditions of Eq.(22) are met within a specified tolerance.

Climb-out trajectories are similarly obtained by a three-parameter search involving the triplet of Eq.(44), attempting to match the initial conditions of Eq.(25) by using backward integration.

Results for Descent and Climb-Out

Results for a trajectory-family of nonturning descent profiles are presented in Figures 7 through 11. The parameters and boundary conditions for the numerical examples are listed in the Appendix.

Figure 7 illustrates the transit time/fuel burn relationship for the nonturning descent trajectory family. It is interesting to note that, since the arrival time is fixed and the system is autonomous, the Hamiltonian along an extremal is a constant. Moreover, this constant can be interpreted as [6]:

$$H^* = \frac{\partial J}{\partial t_f} = \frac{\partial W_F(t_f)}{\partial t_f} \triangleq -CI \qquad (47)$$

That is, H^* can be interpreted as an increment in fuel consumption due to an unit increment in flight time. In other words, the value of H^* is equal to the slope of the time/fuel consumption curve, evaluated at the assigned time. The negative sensitivity of fuel consumption with respect to flight time is often referred to as cost index CI. This parameter also plays an important role in time-free minimum-DOC problems, where CI is a priori specified to represent the ratio of time to fuel cost [5,6]. In Figure 8, the cost index CI is shown as a function of assigned arrival time. Here, CI is expressed in units that are commonly employed in operational practice.

Two points on the curve of Figure 8 are of particular interest. Firstly, the point CI = 0 is of interest, since it corresponds to the minimum-fuel solution in case that the time-of-arrival is not specified. As can be seen from Figure 7, it represents the absolute minimum that can be attained for any assigned arrival time. The second point of interest is the point CI = -136. This point corresponds to the solution with $\lambda_x = 0$, which represents the slowest descent profile that can be obtained without path stretching or holding [4,6].

Figure 9 shows the nonturning descent-family, parameterized by time-of-arrival t_f, in the (V,h)-space. It is observed that some of the faster trajectories "run" into a lower altitude limit. These extremals may also exhibit bank angle chattering when flying along the lower altitude constraint. It is worth noting that both energy and altitude may actually increase during the initial

phase of the descent. This is also illustrated in Figure 10, where the descent flight paths in the vertical plane are shown.

Figure 11 depicts throttle setting as a function of down range. Not surprisingly, the largest initial throttle setting is found for the fastest descent profile. The throttle setting decays gradually with down range, and a substantial fraction of the total range is flown at idle thrust. For trajectories with a positive cost index, this fraction increases as the descent profiles become slower, but decreases for trajectories with a negative cost index.

Results for a trajectory-family of nonturning climb -out profiles are presented in Figures 7 and 12 through 14. The parameters and boundary conditions for the numerical examples are listed in the Appendix.

In Figure 7, the transit time/fuel burn relationship for the nonturning climb-out family is compared with that of the descent trajectory family, for a comparable range of the cost-index. Although the TMA considered in the climb-out calculations is somewhat smaller than the TMA considered in the descent calculations, it is apparent that the time-absorption capability in climb-out is considerable less than in descent.

Figure 12 shows some representative members of the nonturning climb-out family in the (V,h)-space. Extremals with a negative cost index exhibit a somewhat strange behavior. The graphs of throttle setting as a function of range-to-go, shown in Figure 13, may help to explain this behavior. The initial throttle setting (range-to-go = 200 km) is always found to be at its upper limit. As the climb progresses, throttle setting is reduced and gradually decreases towards its level at cruise energy. The throttle setting leaves its limit earlier during the climb if the trajectories become slower, however, for climb-out profiles with a negative cost index, throttle setting may in fact increase again and even run into its upper limit as the climb progresses towards its cruise level. Figure 14 shows some of the nonturning climb-out trajectories in the vertical plane.

In addition to calculating nonturning extremals, we have also performed extensive calculations involving turning trajectories. Figure 15 shows two extremals with the same boundary conditions (including a specified final heading of 150°), but with a different assigned time-of-arrival. The fast trajectory exhibits a substantial altitude variation during the turning phase, which takes place very near to the final energy level. This is even better illustrated in Figure 16, where altitude is shown as a function of heading. It is obvious that the altitude behavior of the fast trajectory is not very realistic. However, it should be realized that such behavior is inherent to energy-state modeling. Since in the energy-state model altitude is a control variable, it is allowed to change instantaneously and this does indeed occur occasionally. Large altitude excursions can be prevented by introducing artificial altitude constraints, but obviously this adversely affects the fuel consumption.

Figure 17 presents bank angle as a function of heading angle for a set of extremals which have the same boundary conditions, but a different assigned time-of-arrival. It is observed that the slower the trajectory, the larger the heading angle at which the bank angle limit is reached.

Figure 18 presents energy as a function of heading for extremals which have the same assigned time-of-arrival and the same boundary conditions, except for final heading, which is specified differently for each extremal shown. It is noted that the curves shown provide simple covering of the region between initial and final energy levels (no point in the considered region has more than one extremal passing through it). This implies that, for a given time-of-arrival, the optimal controls can be uniquely expressed as functions of energy and heading. This is an attractive feature, which may eventually help the development of an on-board feedback guidance system.

One of the possible applications of the present program is to asses the penalties in fuel consumption due to, e.g., the FAA imposed speed constraint of 250 knots IAS on climb-out and descent paths below 10,000 ft. An example in which "constrained" and "unconstrained" extremals are compared, is shown in Figure 19. It's obvious that the magnitude of the fuel penalty increases as the assigned time-of-arrival decreases. In Figure 20 this is illustrated by comparing the fuel consumption of the "unconstrained" nonturning descent solutions of Figure 7, with that of the corresponding "constrained" solutions. Obviously, for slow descent profiles the constraint is never encountered, so that the constrained and unconstrained solutions are identical.

IV. Conclusions

A program has been developed, capable of computing 4D fuel-optimal climb-out and descent trajectories in the Terminal Area. A reduced-order performance model has been used, which considers the important dynamic effects and operational constraints, while significantly reducing the required computational effort.

A field of representative climb-out and descent extremals can be generated in the form of a three-parameter family. Extremals that pass through specified end conditions can be obtained by searching in the three-dimensional parameter-space.

It is emphasized that the extremals are merely candidates for optimality, since they only satisfy the necessary conditions. However, since the amount of heading change is limited to 180°, it is likely that the extremals are also globally optimum.

It is a well-known fact that the calculation of the extremals is very sensitive to the modeling of drag and propulsion system characteristics. For this reason, it is desirable to have some of the current results confirmed by using a different, preferably more detailed, aircraft model.

The observed trajectory-family structure allowed the essential energy management characteristics to be identified. Occasionally, the extremals calculated using the simplified system model, exhibit undesirable features incompatible with operational practice, such as bank angle chattering, rapid (possibly instantaneous) altitude changes, descending turns during climb-out and climbing turns during descent. Although this unrealistic behavior can be modified by introducing additional constraints, this comes at the cost of an increased fuel consumption. The ability to

quantify these performance penalties, is one of the most attractive features of the program.

The insight gained by the present investigations may be beneficially exploited in the development of sub-optimal algorithms that can eventually be implemented on board. The results obtained herein provide standards against which such developments can be evaluated.

Appendix: Numerical Values for Boundary Conditions, Constraints and Model Parameters

In the numerical examples, the modeling approach and numerical values for the Lockheed C-141 Starlifter jet transport of Ref.11 have been adopted. This model is a modified version of the model described in Ref.12.

The drag polar of Ref.12 is modified for two specific reasons. Firstly, to simplify the analysis, the linear term in C_L has been removed from the drag polar. Secondly, the drag polar is modified to account for a low speed configuration (flaps deflected). It is noted that flap setting is not considered as a separate control variable in the present analysis. Instead, flap angle is eliminated from the problem. To this end, for each flap angle the drag coefficient has been computed for the lift coefficient corresponding to V_2. The line connecting these points forms an envelope. Points on this envelope (low speed region) are used in conjunction with points for zero flap deflection (high speed region) to fit the drag polar, yielding:

$$C_D = 0.013 + 8.5 \times 10^{-6}(0.9 - M)^{-2.7} +$$
$$+ \left(0.052 + 9.0 \times 10^{-7}(0.9 - M)^{-4.6}\right)C_L^2 \quad \text{(A.1)}$$

The fuel flow model of Ref.12 has been modified as well. The reason for this is that Ref.12 employs a separate fuel flow model for idle thrust. To ensure smooth fuel flow modeling, a "composite" model is used here which is the average of the two models of Ref.12:

$$\sigma_{total} = \left(0.505 + 0.382 \times TN + 0.248 \times M +\right.$$
$$+ 0.0096 \times TN^2 + 0.346 \times TN \times M +$$
$$\left. + 1.477 \times M^2\right)\delta\sqrt{\theta} \quad \text{(kg/s)} \quad \text{(A.2)}$$

where:

$$TN = T_e/(6100\delta) \quad \text{(A.3)}$$

and T_e is the thrust in N/engine (the C-141 has four engines). The maximum thrust per engine (normal rated thrust) is parameterized as:

$$TH_{max} = 1000 \left(77.57 - 68.23 \times H - 63.25 \times M + \right.$$
$$+ 0.178 \times H^2 + 81.62 \times H \times M + 42.79 \times M^2 -$$
$$\left. - 2.62 \times H^2 \times M - 52.53 \times H \times M^2 + 3.34 \times H^2 \times M^2\right)$$
$$= T_{max}(M,h)/4 \quad \text{(N)} \quad \text{(A.4)}$$

$$H = h/12200 \quad \text{(m)} \quad \text{(A.5)}$$

The minimum normal rated thrust (idle thrust) per engine is represented by:

$$TH_{min} = 100 \left(49.95 - 78.02 \times H - 75.35 \times M + \right.$$
$$+ 68.32 \times H^2 + 138.69 \times H \times M - 80.95 \times M^2 -$$
$$\left. - 75.62 \times H^2 \times M + 61.38 \times H \times M^2 - 11.12 \times H^2 \times M^2\right)$$
$$= T_{min}(M,h)/4 \quad \text{(N)} \quad \text{(A.6)}$$

Some other aircraft model parameters are:

$$W = 1145416.7 \text{ N} \text{ , } S = 299.9 \text{ m}^2 \quad \text{(A.7)}$$

The numerical values for the constraints are:

$$h_T = 0 \text{ m} \text{ , } q_{MO} = 27269.113 \text{ N/m}^2 \text{ , } M_{MO} = 0.83$$
$$C_{L_{max}} = 1.6 \text{ , } \mu_{max} = 30° \quad \text{(A.8)}$$

The numerical values for the boundary conditions in the descent examples are:

$$E_{cr} = 12131 \text{ m} \text{ , } E_f = 1500 \text{ m} \text{ , } R = 250 \text{ km} \quad \text{(A.9)}$$

Similarly, the boundary conditions in the climb-out examples are:

$$E_{cr} = 12131 \text{ m} \text{ , } E_0 = 1500 \text{ m} \text{ , } R = 200 \text{ km} \quad \text{(A.10)}$$

References

[1] Lee, H. Q., Hardy, G.H., "4-D Area Navigation System Description and Flight Test Results," NASA TN-D7874, 1975.

[2] Kelley, H.J., "Aircraft Maneuver Optimization by Reduced Order Approximations," Advances in Control and Dynamic Systems, Vol.10, Academic Press, New York, 1973, pp.131-178.

[3] Erzberger, H. and Lee, H., "Constrained Optimum Trajectories with Specified Range," Journal of Guidance and Control, Vol.3, Jan.-Feb. 1980, pp. 78-85.

[4] Sorensen, J.A., Waters, M.H. "Airborne Method to Minimize Fuel with Fixed Time-of-Arrival Constraints," Journal of Guidance and Control, Vol.4, May-June 1981, pp. 348-349.

[5] Burrows, J.W., "Fuel-Optimal Aircraft Trajectories with Fixed Arrival Times," Journal of Guidance and Control, Vol.6, Jan.-Feb. 1983, pp. 78-85.

[6] Chakravarty, A., "Four-Dimensional Fuel-Optimal Guidance in the Presence of Winds," Journal of Guidance and Control, Vol.8, Jan.-Feb. 1985, pp. 16-22.

[7]Neuman, F. and Kreindler, E., "Minimum-Fuel Three-Dimensional Flightpath Guidance of Transport Jets," " Journal of Guidance and Control, Vol.8, Sept.-Oct. 1985, pp. 650-657.

[8]Kreindler, E. and Neuman, F., "Minimum-Fuel Three-Dimensional Flight Paths for Jet Transports," NASA TP 2326, 1984.

[9]Benoit, A., Swierstra S., "A Minimum Fuel Transit Procedure for the Control of Inbound Traffic," Eurocontrol Doc. No. 802007, April 1980.

[10]Rajan, N., Ardema, M.D.,"Interception on Three Dimensions: An Energy Formulation," Journal of Guidance and Control, Vol.8, Jan.-Feb. 1985, pp. 23-30.

[11]Westerbeek, R., "Four-Dimensional Fuel-Optimal Descents in the Terminal Area," Master Thesis, Delft University of Technology, Delft, The Netherlands, August 1988.

[12]Aggarwal, R., Calise, A.J. and Goldstein, F., "Singular Perturbation Analysis of Optimal Flight Profiles for Transport Aircraft," JAC Conference, San Francisco, June 1977.

[13]Bryson, A.E., Ho, Y.-C., "Applied Optimal Control", Hemisphere Publishing Corporation, Washington, 1975.

[14]Visser, H.G., Kelley, H.J. and Cliff, E.M., "Energy Management of Three Dimensional Minimum Time Intercept," J.Guidance, Control and Dynamics, Vol.10, Nov.-Dec. 1987, pp.574-580.
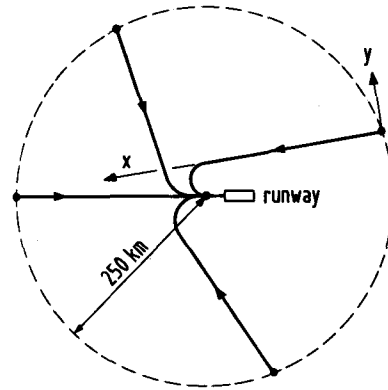
Fig. 2 Sample Descent Flight Paths in the TMA.
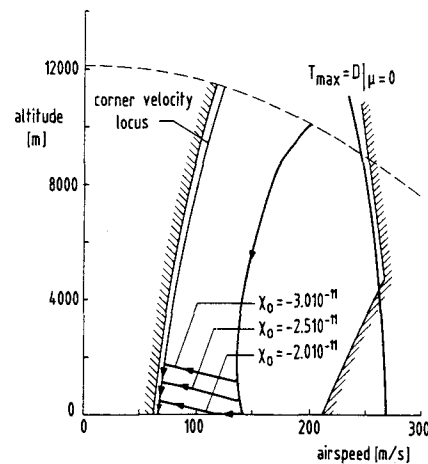
Fig. 3 Descent Extremals in the (V,h)-space.
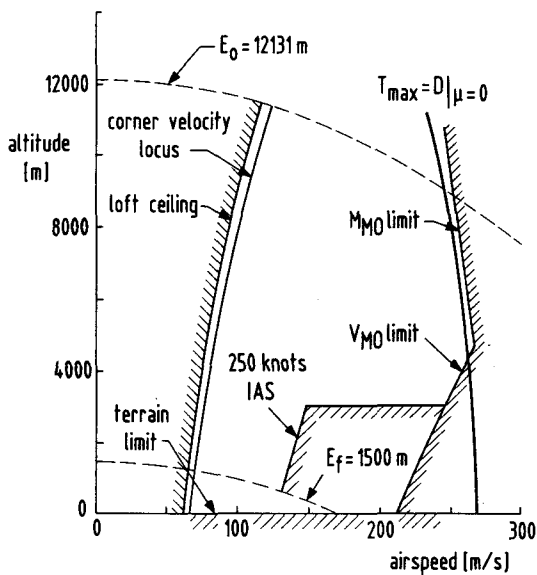
Fig. 1 Constraints in the (V,h)-space.
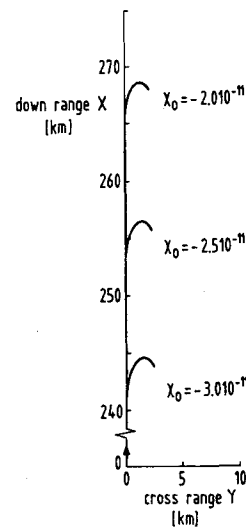
Fig. 4 Ground Tracks of Descent Extremals.

1475
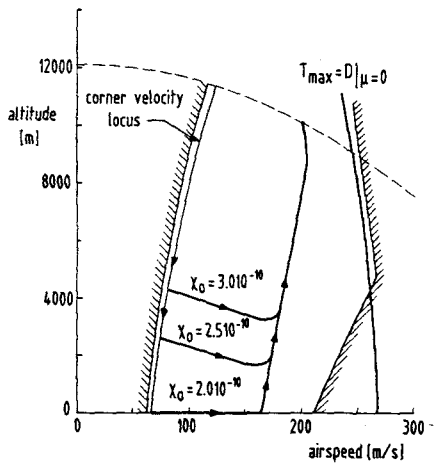
Fig. 5 Climb-Out Extremals in the (V,h)-space.
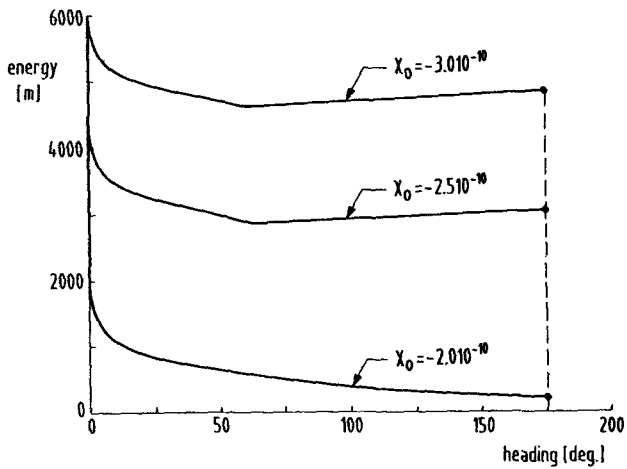
Fig. 6 Climb-Out Extremals in the (X,E)-space

Fig. 7 Transit Fuel Consumption as a Function of
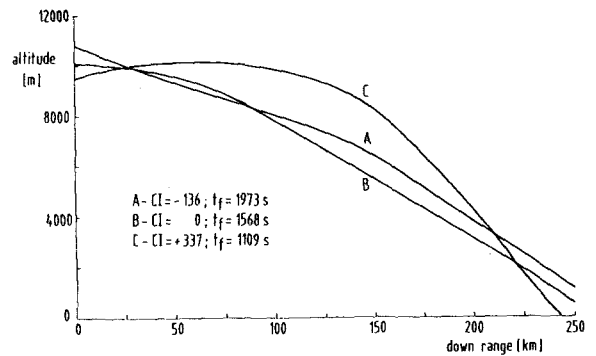Transit Time for Nonturning Climb-out and
Descent Trajectories.
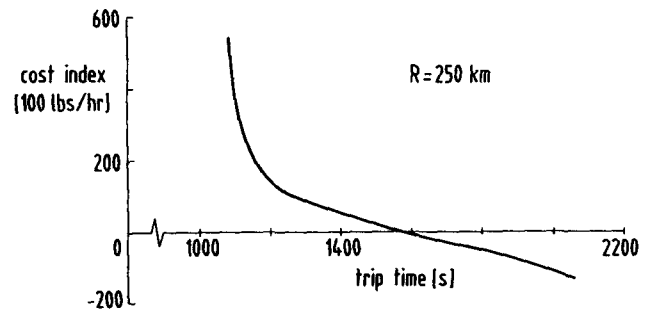
Fig. 8 Cost Index as a Function of Transit Time
for Nonturning Descent Trajectories.
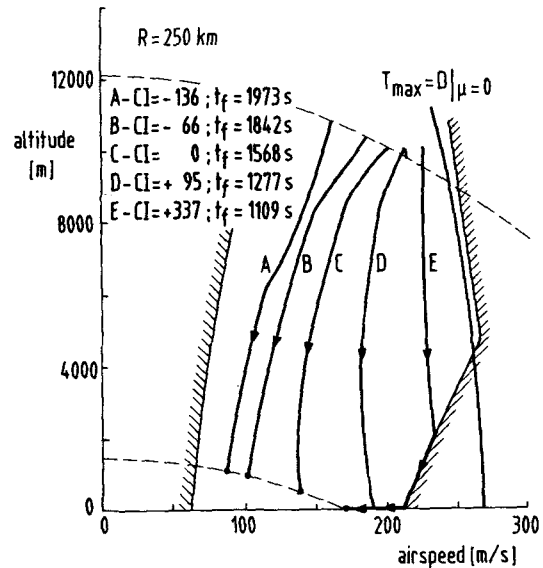
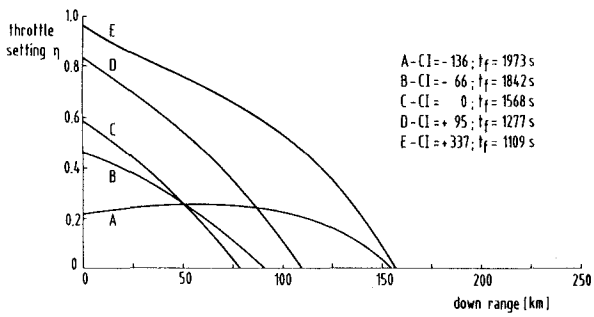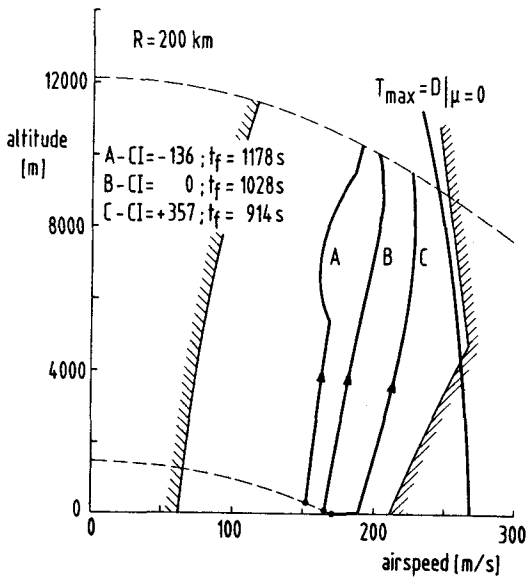Fig. 9 A Family of Nonturning Descent Trajectories
in the (V,h)-space.

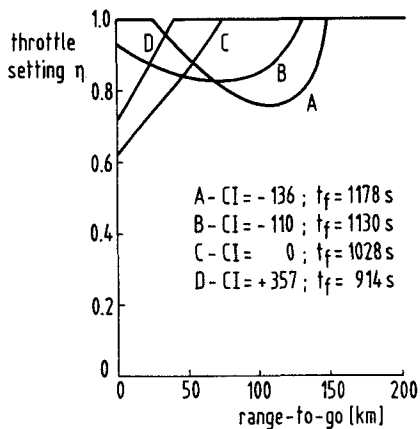Fig. 10 A Family of Nonturning Descent
Trajectories in the Vertical Plane.

Fig. 11 Throttle Setting as a Function of Down
Range for a Family of Nonturning Descent
Trajectories.
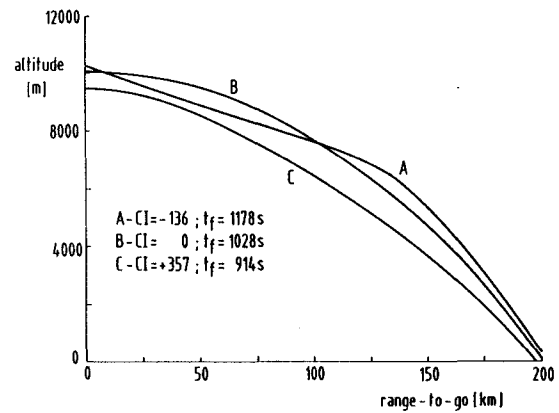
Fig. 12 A Family of Nonturning Climb-Out
Trajectories in the (V,h)-space.

Fig. 13 Throttle Setting as a Function of
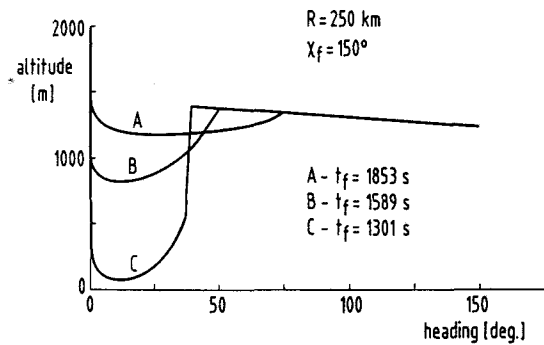Range-to-go for a Family of Nonturning
Climb-Out Trajectories.

Fig. 14 A Family of Nonturning Climb-Out
Trajectories in the Vertical Plane.

Fig. 15 A Family of Turning Descent Trajectories
in the (V,h)-space.

Fig. 16 Altitude as a Function of Heading for a
Family of Turning Descent Trajectories.

1477
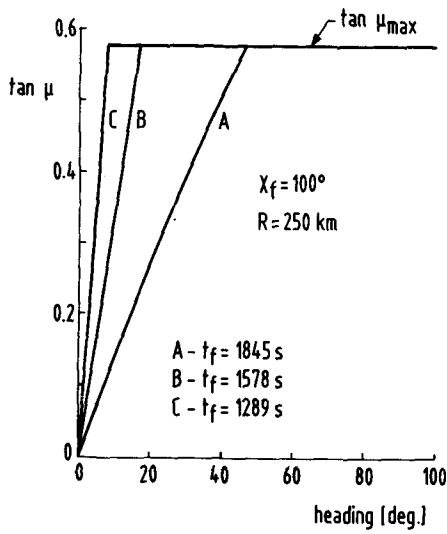
Fig. 17 Bank Angle as a Function of Heading for a
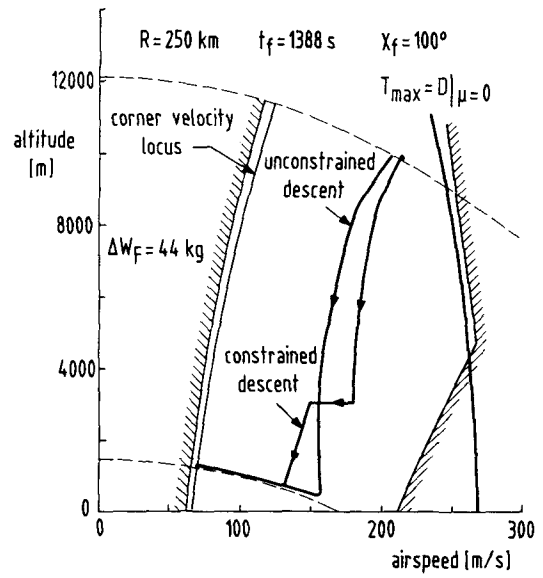Family of Turning Descent Trajectories.

Fig. 19 A Comparison of Turning Constrained and
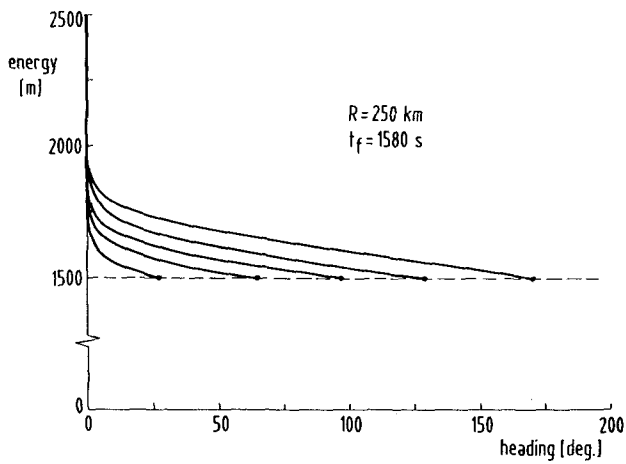Unconstrained Descent Solutions in the
(V,h)-space.

Fig. 18 A Family of Turning Descent Trajectories
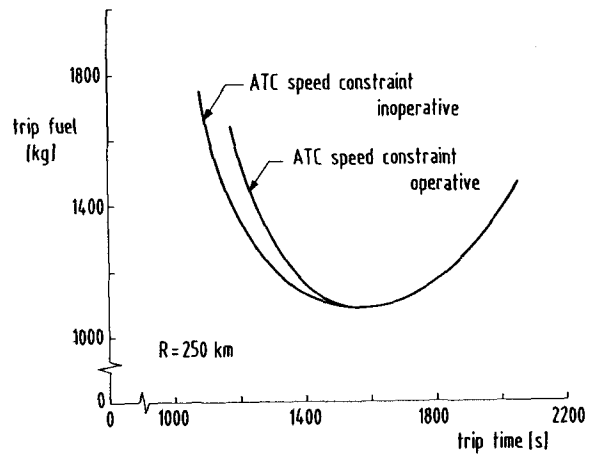in the (X,E)-space.

Fig. 20 Transit Fuel Consumption as a Function of
Transit Time for Nonturning Constrained
and Unconstrained Descent Trajectories.